ARCHIVES OF ELECTRICAL ENGINEERING VOL. 69(4), pp. 891–905 (2020)

DOI 10.24425/aee.2020.134637

Harmonic mitigation in 18-pulse rectifier based on zigzag autotransformer by DC side auxiliary circuit

JIONGDE LIU [1], XIAOQIANG CHEN [1, 2], YING WANG [1], TAO CHEN [1]

[1] *School of Automation and Electrical Engineering, Lanzhou Jiaotong University China*

[2] *Key Laboratory of Opto-Electronic Technology and Intelligent Control Ministry of Education, Lanzhou Jiaotong University China*

e-mail: xliujdx@163.com

(Received: 12.04.2020, revised: 18.06.2020)

Abstract: To improve the power quality of a multi-pulse rectifier, a zigzag 18-pulse uncontrolled rectifier with an auxiliary circuit at the DC side is proposed. When the grid-side currents are sinusoidal waves, the required DC side injection currents to be compensated can be obtained by analyzing the AC-DC side relationship of diode bridge rectifiers. Then the 6 compensation currents generated by an active auxiliary circuit are injected into the DC side to eliminate the grid-side harmonics of the rectifier. The simulation results verifying the correctness of the theoretical analysis show that the proposed rectifier can mitigate the harmonic content, as the total harmonic distortion of the grid-side current is about 1.45%. In addition, the single-phase inverter used in the active auxiliary circuit has the characters of simple circuit structure and easy controllability.

Key words: 18-pulse rectifier, harmonic suppressing, zigzag autotransformer

1. Introduction

A multi-pulse rectifier is a widely used power converter in industrial engineering such as in aerospace, an urban rail power supply system, metallurgy field [1–3]. However, due to the nonlinearity of the rectifier, harmonics are generated in power grids [4]. How to mitigate the grid-side harmonic content of a multi-pulse rectifier has been one of the research hotspots of multi-pulse rectifier technology [5, 6].

The grid-side current harmonics can be suppressed by increasing the pulse number of an output current waveform at the DC side of the multi-pulse rectifier. For instance, under the condition of large inductive load, the total harmonic distortion (THD) value of a 12-pulse rectifier grid-side current is 15.2% [7] and that of an 18-pulse rectifier is 7.36% [8], but neither of the two values can meet the standard for the rectifier to connect to a power grid. However, simply increasing the pulse number will make the manufacturing of phase-shifting transformers difficult [9].

As for the multi-pulse rectifier with a lower number of pulses, the application of an injection circuit with active currents on the DC side is economical and effective. In [10], a boost converter is installed at the secondary side of the inter-phase reactor of a 12-pulse rectifier to generate triangular loop currents, which can decrease the THD of the grid-side current of the rectifier to 2.64%, approximately. References [11, 12] have improved the DC side by adding a zero-sequence current suppressor to deliver the power supply to the active inverter from the load. In [13], a method using an active inter-phase reactor to suppress the input current harmonics is presented for the large current rectifier based on a star-connected autotransformer. In this method, the output currents of two sets of three phase bridges can be changed by controlling the input current of the auxiliary circuit to make the grid-side currents sinusoidal. A novel DC side active filter for a wind turbine is proposed, which combines a 12-pulse polygon rectifier with a dual-buck full-bridge inverter to make the whole system have the characteristics of low harmonic distortion and high reliability [14].

A zigzag autotransformer has the characteristics of a simple structure and small capacity [15]. It can be used not only as a grounding transformer in a power distribution system [16], but also as a phase-shifting transformer in a multi-pulse rectifier system. Furthermore, due to the unique characteristic of the zigzag transformer, it can block the zero-sequence current, so the zero sequence blocking transformer can be omitted in the rectifier based on the zigzag transformer [17], thereby reducing the equivalent capacity of the system further.

In order to suppress the grid-side current harmonics of the 18-pulse rectifier, a rectifier based on a zigzag autotransformer with an auxiliary circuit on the DC side is proposed. The active circuit generates 6 compensation currents directly injected into the positive and negative ports of the three groups of diode bridge rectifiers (DBRs) to decrease the grid-side harmonic content without changing any component structure of the original rectifying circuit.

2. Operation principle of the proposed rectifier

2.1. Topology of 18-pulse rectifier

Fig. 1 shows the schematic diagram of the proposed 18-pulse rectifier with an auxiliary circuit at the DC side. The proposed rectifier consists of three-phase voltage sources, an improved zigzag phase-shifting autotransformer, the inter-phase reactors (IPRs), an auxiliary circuit and three groups of DBRs, namely DBR I, DBR II and DBR III. The instantaneous voltage difference between the three groups of DBRs can be absorbed by the IPRs to let the DBRs work independently.

In Fig. 1, $\dot{V}_a$, $\dot{V}_b$, $\dot{V}_c$, are the input phase voltages of the autotransformer. The i_{x1}^{+}, i_{x2}^{+}, i_{x3}^{+} and i_{x1}^{-}, i_{x2}^{-}, i_{x3}^{-} are the specific compensating currents generated by the active auxiliary circuit. In addition, The i_a, i_b, i_c represent the grid-side currents, the currents i_{a1}, i_{b1}, i_{c1}, i_{a2}, i_{b2}, i_{c2} and

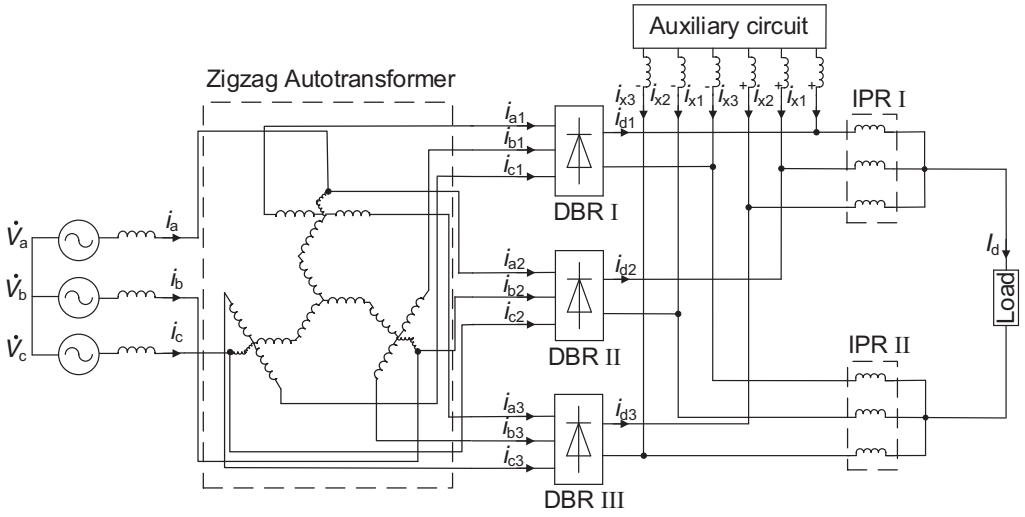

Fig. 1. Main circuit of the zigzag 18-pulse rectifier with an auxiliary circuit at the DC side

i_{a3}, i_{b3}, i_{c3} are the three-phase input currents of the three groups of DBRs. I_d is the output load current and i_{d1}, i_{d2}, i_{d3} are the output currents of the DBRs.

2.2. Winding design of zigzag autotransformer

In order to make the pulse number of the DC side output current waveform be 18, the windings of the zigzag phase-shifting transformer need to be designed. Fig. 2 shows the voltage phasor-diagram of the 18-pulse zigzag autotransformer. $\dot{V}_{a1}$, $\dot{V}_{b1}$, $\dot{V}_{c1}$, $\dot{V}_{a2}$, $\dot{V}_{b2}$, $\dot{V}_{c2}$ and $\dot{V}_{a3}$, $\dot{V}_{b3}$, $\dot{V}_{c3}$ are the output phase voltages of the transformer. The angle α is the phase-shifting angle of output voltages of the transformer.

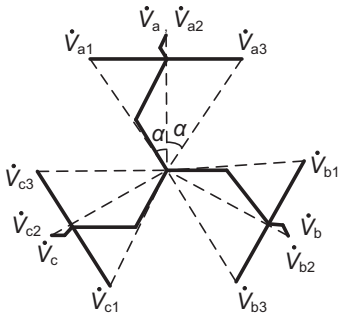

Fig. 2. Voltage phasor-diagram of 18-pulse zigzag autotransformer

The input phase voltages and the input line voltages of the rectifier are given as in:

$$\begin{cases} \dot{V}_{\mathrm{a}} = \dot{V}_{\mathrm{a2}} = V_s \angle 0^\circ \\ \dot{V}_{\mathrm{b}} = \dot{V}_{\mathrm{b2}} = V_s \angle -120^\circ \\ \dot{V}_{\mathrm{c}} = \dot{V}_{\mathrm{c2}} = V_s \angle 120^\circ \end{cases}, \tag{1}$$

$$\begin{cases} \dot{V}_{\mathrm{ab}} = \sqrt{3} V_s \angle 30^\circ \\ \dot{V}_{\mathrm{bc}} = \sqrt{3} V_s \angle -90^\circ \\ \dot{V}_{\mathrm{ca}} = \sqrt{3} V_s \angle 150^\circ \end{cases}, \tag{2}$$

where V_s is the rms value of phase voltages.

The zigzag transformer of the 18-pulse rectifier shall provide three groups of voltages with a phase displacement of 20° [9], so the α is 20° and here come the formulas:

$$\dot{V}_{\mathrm{a1}} = V \angle 20^\circ, \quad \dot{V}_{\mathrm{b1}} = V \angle -100^\circ, \quad \dot{V}_{\mathrm{c1}} = V \angle 140^\circ, \tag{3}$$

$$\dot{V}_{\mathrm{a3}} = V \angle -20^\circ, \quad \dot{V}_{\mathrm{b3}} = V \angle -140^\circ, \quad \dot{V}_{\mathrm{c3}} = V \angle 100^\circ, \tag{4}$$

where V is the rms value of output phase voltages of the phase-shifting transformer.

In Fig. 3, the transformation ratios K_1, K_2 and K_3 of a phase-shifting autotransformer are set. Then by Fig. 2, we can get:

$$V_s = V, \tag{5}$$

$$\dot{V}_{\mathrm{a1}} = K_1 \left(\dot{V}_{\mathrm{ab}} - \dot{V}_{\mathrm{ca}} \right) - K_2 \dot{V}_{\mathrm{bc}}, \tag{6}$$

$$\dot{V}_{\mathrm{a3}} = K_1 \left(\dot{V}_{\mathrm{ab}} - \dot{V}_{\mathrm{ca}} \right) + K_2 \dot{V}_{\mathrm{bc}}, \tag{7}$$

$$\dot{V}_{\mathrm{a}} = \dot{V}_{\mathrm{a2}} = K_1 \left(\dot{V}_{\mathrm{ab}} - \dot{V}_{\mathrm{ca}} \right) + K_3 \left(\dot{V}_{\mathrm{ab}} - \dot{V}_{\mathrm{ca}} \right). \tag{8}$$

From (1)–(8), the winding turn ratios can be obtained as $K_1 = 0.31323$, $K_2 = 0.1975$, $K_3 = 0.0201$.

2.3. Theoretical analysis of injected currents

Fig. 3 shows the winding configuration of a zigzag phase-shifting autotransformer. According to the currents relationship in Fig. 1, we can set the compensating currents i_{x1}, i_{x2}, i_{x3} as in (9) by Kirchhoff's Current Law (KCL). In Fig. 3, currents i_1, i_2, i_3 represent the currents in the windings of the phase-shifting transformer. Similarly, by applying KCL, currents i_{a}, i_{b}, i_{c} can be expressed in (10).

$$\begin{cases} i_{\mathrm{x1}} = i_{\mathrm{x1}}^{+} = -i_{\mathrm{x1}}^{-} \\ i_{\mathrm{x2}} = i_{\mathrm{x2}}^{+} = -i_{\mathrm{x2}}^{-} \\ i_{\mathrm{x3}} = i_{\mathrm{x3}}^{+} = -i_{\mathrm{x3}}^{-} \end{cases}, \tag{9}$$

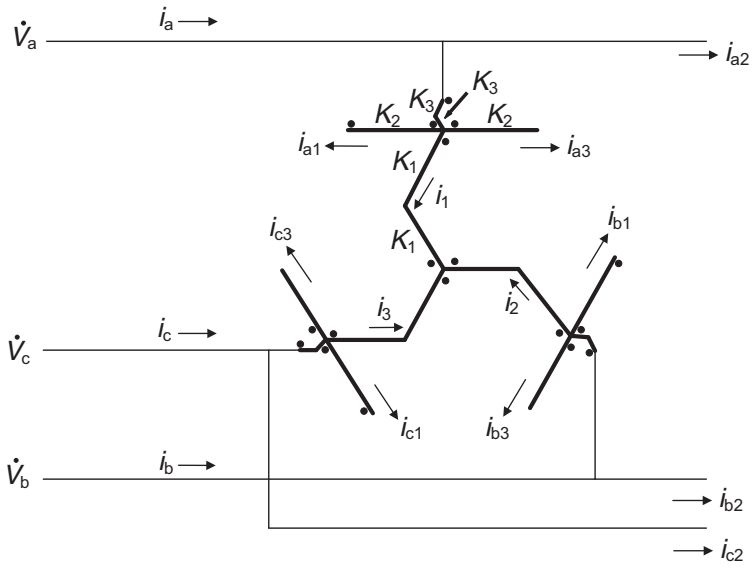

Fig. 3. Winding configuration of 18-pulse zigzag autotransformer

$$\begin{cases} i_a = i_{a1} + i_{a2} + i_{a3} + i_1 \\ i_b = i_{b1} + i_{b2} + i_{b3} + i_1 \\ i_c = i_{c1} + i_{c2} + i_{c3} + i_1 \\ i_d = i_1 + i_2 + i_3 + i_1 \end{cases} . \tag{10}$$

The balance relationship of Magneto Motive Force (MMF) of the zigzag autotransformer is as follows:

$$\begin{cases} K_1(i_2 - i_3) + K_2(i_{a1} - i_{a3}) - K_3(i_c - i_{c2} - i_b + i_{b2}) = 0 \\ K_1(i_3 - i_1) + K_2(i_{b1} - i_{b3}) - K_3(i_a - i_{a2} - i_c + i_{c2}) = 0 \\ K_1(i_1 - i_2) + K_2(i_{c1} - i_{c3}) - K_3(i_b - i_{b2} - i_a + i_{a2}) = 0 \end{cases} . \tag{11}$$

By (10)–(11), the relationship between the grid-side currentsi_a, i_b, i_c and the output currents i_{a1}, i_{b1}, i_{c1}, i_{a2}, i_{b2}, i_{c2} and i_{a3}, i_{b3}, i_{c3} of the autotransformer can be calculated as in:

$$\begin{cases} i_a = \dfrac{3K_1\,(i_{a1}+i_{a2}+i_{a3}) + K_2\,(i_{b1}-i_{b3}-i_{c1}+i_{c3}) + K_3\,(i_{a1}+i_{a3}+i_{b1}+i_{b3}+i_{c1}+i_{c3}+3i_{a2})}{3(K_1+K_3)} \\ i_b = \dfrac{3K_1\,(i_{b1}+i_{b2}+i_{b3}) + K_2\,(i_{c1}-i_{c2}-i_{c3}+i_{a3}) + K_3\,(i_{a1}+i_{a3}+i_{b1}+i_{b3}+i_{c1}+i_{c3}+3i_{b2})}{3(K_1+K_3)} \\ i_c = \dfrac{3K_1\,(i_{c1}+i_{c2}+i_{c3}) + K_2\,(i_{a1}-i_{a3}-i_{b1}+i_{b3}) + K_3\,(i_{a1}+i_{a3}+i_{b1}+i_{b3}+i_{c1}+i_{c3}+3i_{c2})}{3(K_1+K_3)} \end{cases} . \tag{12}$$

The relation between the input and output sides of the DBRs can be expressed by introducing the switching function. Therefore, the grid-side currents can be presented by the switching

function and the output currents of the DBRs. The input currents of the DBRs can be expressed as in:

$$\begin{bmatrix} i_{a1} & i_{a2} & i_{a3} \\ i_{b1} & i_{b2} & i_{b3} \\ i_{c1} & i_{21} & i_{c3} \end{bmatrix} = \begin{bmatrix} S_{a1}i_{d1} & S_{a2}i_{d2} & S_{a3}i_{d3} \\ S_{b1}i_{d1} & S_{b2}i_{d2} & S_{b3}i_{d3} \\ S_{c1}i_{d1} & S_{c2}i_{d2} & S_{c3}i_{d3} \end{bmatrix}, \tag{13}$$

where $S_{a1}(t)$, $S_{b1}(t)$, $S_{c1}(t)$, $S_{a2}(t)$, $S_{b2}(t)$, $S_{c2}(t)$ and $S_{a3}(t)$, $S_{b3}(t)$, $S_{c3}(t)$ are the switching functions of phase a_1, phase b_1, phase c_1, phase a_2, phase b_2, phase c_2 and phase a_3, phase b_3, phase c_3.

Meanwhile, by applying KCL in Fig. 1, output currents i_{d1}, i_{d2}, i_{d3} of the DBRs can be expressed as in (14):

$$\begin{bmatrix} i_{d1} \\ i_{d2} \\ i_{d3} \end{bmatrix} = \begin{bmatrix} \frac{I_d}{3} - i_{x1} \\ \frac{I_d}{3} - i_{x2} \\ \frac{I_d}{3} - i_{x3} \end{bmatrix}. \tag{14}$$

Substitute (13) and (14) into (12), the grid-side currents expressed by DC load current I_d and injected compensating currents i_{x1}, i_{x2}, i_{x3} can be written as in:

$$\begin{cases} A = -A_1 i_{x1} - A_2 i_{x2} - A_3 i_{x3} \\ B = -B_1 i_{x1} - B_2 i_{x2} - B_3 i_{x3} \\ C = -C_1 i_{x1} - C_2 i_{x2} - C_3 i_{x3} \end{cases}, \tag{15}$$

where:

$$\begin{aligned} A &= i_a - \frac{I_d}{3}(A_1 + A_2 + A_3), \\ A_1 &= (3K_1 + K_3) S_{a1} + (K_2 + K_3) S_{b1} + (K_3 - K_2) S_{c1}, \\ A_2 &= (3K_1 + 3K_3) S_{a2}, \\ A_3 &= (3K_1 + K_3) S_{a3} + (K_3 - K_2) S_{b3} + (K_2 + K_3) S_{c3}, \\ B &= i_b - \frac{I_d}{3}(B_1 + B_2 + B_3), \\ B_1 &= (K_3 - K_2) S + (3K_1 + K_3) S_{b1} + (K_2 + K_3) S_{c1}, \\ B_2 &= (3K_1 + 3K_3) S_{b2}, \\ B_3 &= (K_2 + K_3) S_{a3} + (3K_1 + K_3) S_{b3} + (K_3 - K_2) S_{c3}, \\ C &= i_c - \frac{I_d}{3}(C_1 + C_2 + C_3), \\ C_1 &= (K_2 + K_3) S_{a1} + (K_3 - K_2) S_{b1} + (3K_1 + K_3) S_{c1}, \\ C_2 &= (3K_1 + 3K_3) S_{c2}, \\ C_3 &= (K_3 - K_2) S_{a3} + (K_2 + K_3) S_{b3} + (3K_1 + K_3) S_{c3}. \end{aligned}$$

To ensure the complete compensation of the rectifying system, the grid-side currents i_a, i_b, i_c are set as in:

$$\begin{cases} i_a = \dfrac{2\sqrt{3}}{\pi} I_d \sin(\omega t) \\ i_b = \dfrac{2\sqrt{3}}{\pi} I_d \sin\left(\omega t - \dfrac{2\pi}{3}\right) \\ i_c = \dfrac{2\sqrt{3}}{\pi} I_d \sin\left(\omega t + \dfrac{2\pi}{3}\right) \end{cases}. \tag{16}$$

Directly solving (15) shows that the numerators and denominators of i_{x1}, i_{x2} and i_{x3} are all zero, so the equation has no solution. Then using the Superposition Theorem to solve (15).

Let the $i_{x1} = 0$, $i_{x2} = i_{x21}$, $i_{x3} = i_{x31}$, then

$$\begin{cases} B_2 i_{x21} + B_3 i_{x31} + B = 0 \\ C_2 i_{x21} + C_3 i_{x31} + C = 0 \end{cases}. \tag{17}$$

Let the $i_{x2} = 0$, $i_{x1} = i_{x11}$, $i_{x3} = i_{x32}$, then

$$\begin{cases} A_1 i_{x11} + A_3 i_{x32} + A = 0 \\ C_1 i_{x11} + C_3 i_{x32} + C = 0 \end{cases}. \tag{18}$$

Let the $i_{x3} = 0$, $i_{x1} = i_{x12}$, $i_{x2} = i_{x22}$, then

$$\begin{cases} A_1 i_{x12} + A_2 i_{x22} + A = 0 \\ B_1 i_{x12} + B_2 i_{x22} + B = 0 \end{cases}. \tag{19}$$

In the three cases above, the injected currents shall compensate 1/3 of the total harmonic currents. The purpose of full compensation can be achieved through the superposition of the three cases. Therefore, the i_{x1}, i_{x2}, i_{x3} can be expressed as follows:

$$\begin{cases} i_{x1} = \dfrac{i_{x11} + i_{x12}}{3} \\ i_{x2} = \dfrac{i_{x21} + i_{x22}}{3} \\ i_{x3} = \dfrac{i_{x31} + i_{x32}}{3} \end{cases}. \tag{20}$$

From (15) and (17)–(20), the compensating currents i_{x1}, i_{x2}, i_{x3} can be calculated as in:

$$\begin{cases} i_{x1} = \dfrac{1}{3}\left(\dfrac{A_2 B - A B_2}{A_1 B_2 - A_2 B_1} + \dfrac{A_3 C - A C_3}{A_1 C_3 - A_3 C_1}\right) \\ i_{x2} = \dfrac{1}{3}\left(\dfrac{A B_1 - A_1 B}{A_1 B_2 - A_2 B_1} + \dfrac{B_3 C - B C_3}{B_2 C_3 - B_3 C_2}\right) \\ i_{x3} = \dfrac{1}{3}\left(\dfrac{A C_1 - A_1 C}{A_1 C_3 - A_3 C_1} + \dfrac{B C_2 - B_2 C}{B_2 C_3 - B_3 C_2}\right) \end{cases}. \tag{21}$$

The expressions of the compensating currents are complex and not easy to implement in practice. Therefore, calculating (21) by MATLAB, we can approximately obtain the waveforms of the ratios of compensating currents i_{x1}, i_{x2}, i_{x3} to DC side load current I_d, as shown in Fig. 4, in which, the waveforms of i_{x1}/I_d, i_{x2}/I_d and i_{x3}/I_d are the same but with a phase displacement of 20°. Under the condition of power frequency, the waveform shown in Fig. 4 can be injected into the DC side in the rectifier to make the grid-side current waveform closer to a sinusoidal wave.

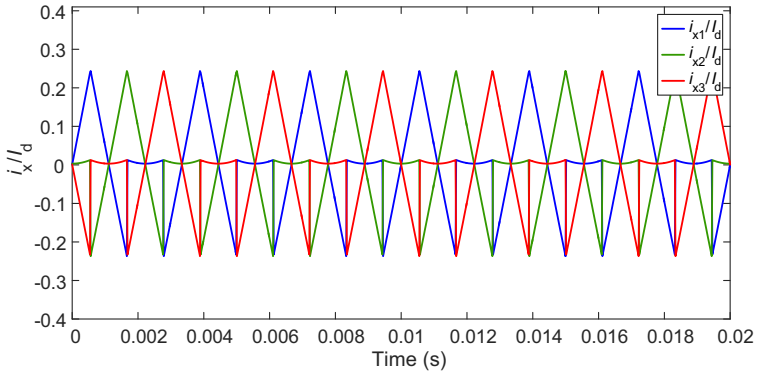

Fig. 4. Theoretical compensating waveforms of i_x/I_d

3. Implementation of injection at DC side

To generate the current waveform i_{x1}/I_d in Fig. 4 easily, we replace the waveform by the simplified waveform in Fig. 5 with a frequency of 300 Hz, that is, a period of 1/300 s and an amplitude of $0.2437I_d$. The waveforms of i_{x2}/I_d and i_{x3}/I_d are 20°, 40° out of the phase with i_{x1}/I_d. Therefore, the triangular waves in Fig. 6 shall be properly selected to generate the simplified waveforms. The relationship between the injected currents i_{x1}, i_{x2} and i_{x3} and the triangular wave currents i_{tri1} and i_{tri2} should be expressed as in:

$$i_{x1} = \begin{cases} i_{tri1} & t \in \left(\dfrac{kT_0}{3} - \dfrac{T_0}{36}, \dfrac{kT_0}{3} + \dfrac{T_0}{12}\right) \\ 0 & t \in \left(\dfrac{kT_0}{3} + \dfrac{T_0}{12}, \dfrac{kT_0}{3} + \dfrac{5T_0}{36}\right) \\ i_{tri2} & t \in \left(\dfrac{kT_0}{3} + \dfrac{5T_0}{36}, \dfrac{kT_0}{3} + \dfrac{T_0}{4}\right) \end{cases},$$

$$i_{x2} = \begin{cases} i_{tri1} & t \in \left(\dfrac{kT_0}{3} + \dfrac{7T_0}{36}, \dfrac{kT_0}{3} + \dfrac{11T_0}{36}\right) \\ 0 & t \in \left(\dfrac{kT_0}{3} + \dfrac{5T_0}{36}, \dfrac{kT_0}{3} + \dfrac{7T_0}{36}\right) \\ i_{tri2} & t \in \left(\dfrac{kT_0}{3} + \dfrac{T_0}{36}, \dfrac{kT_0}{3} + \dfrac{5T_0}{36}\right) \end{cases}, \tag{22}$$

$$i_{x3} = \begin{cases} i_{tri1} & t \in \left(\dfrac{kT_0}{3} + \dfrac{T_0}{12}, \dfrac{kT_0}{3} + \dfrac{7T_0}{36} \right) \\ 0 & t \in \left(\dfrac{kT_0}{3} + \dfrac{T_0}{36}, \dfrac{kT_0}{3} + \dfrac{T_0}{12} \right) \\ i_{tri2} & t \in \left(\dfrac{kT_0}{3} - \dfrac{T_0}{12}, \dfrac{kT_0}{3} + \dfrac{T_0}{36} \right) \end{cases},$$

where: $T_0 = 0.02$ s, k is an integer.

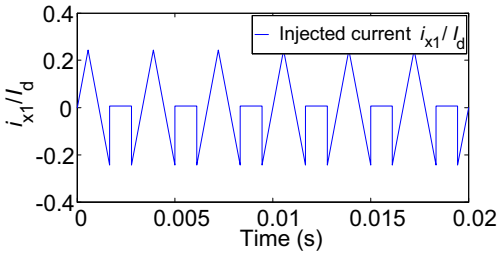

Fig. 5. Simplified injection current i_{x1}/I_d

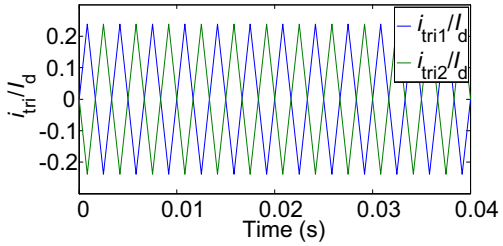

Fig. 6. Required triangular waveforms

Fig. 7 and Fig. 8 show the structure of the DC side active auxiliary circuit and the control scheme of the inverter, respectively. The current hysteresis-band control method is adopted to

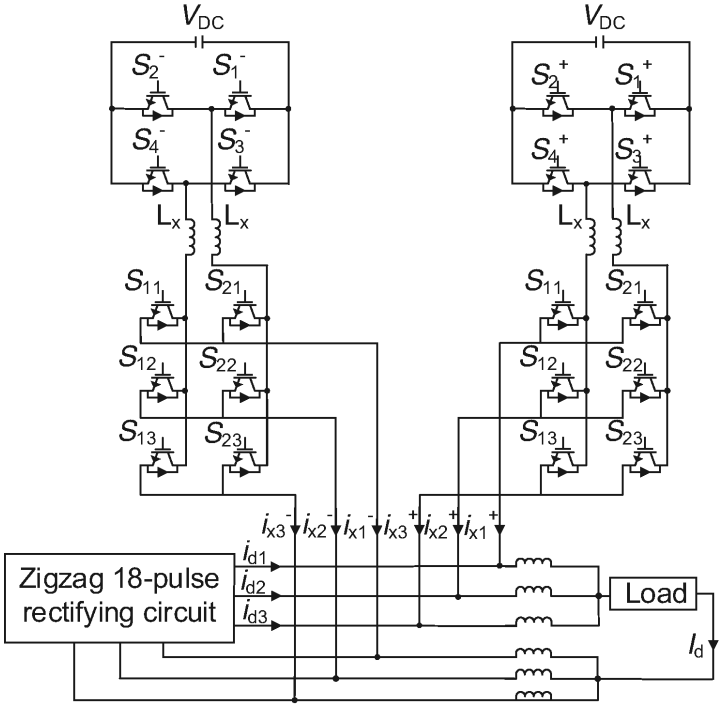

Fig. 7. Active auxiliary circuit

generate the required triangular waveform. This control method is easy to realize and it is closed-loop control with strong stability. Fig. 8 shows the control schematic graph of the inverter.

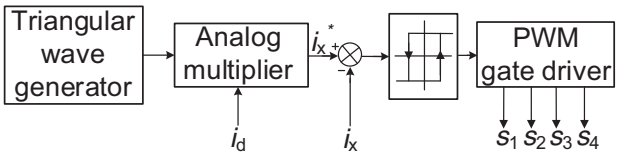

Fig. 8. Control block diagram of the inverter

The triangular wave generator produces a triangular wave with 6 times the power frequency and an amplitude of ±0.2437. By comparing the reference current of the multiplier with the current generated by the inverter, the difference signal is connected to the hysteresis controller. After the hysteresis controller generates the driving signal to drive a single-phase inverter, the required 6 times power frequency triangular currents which can change with the load current I_d can be obtained. Then selecting the required triangular currents by corresponding switch combinations can get the simplified injection currents to compensate the 18-pulse rectifying system.

4. Validation and results

In MATLAB/Simulink, the simulation model of the proposed 18-pulse zigzag auto-coupled transformer rectifying system based on DC side active harmonic suppression technology is established with an input line voltage of 380 V and an output DC voltage of 510 V. Fig. 9(a) and Fig. 9(b) are the simulation models of the zigzag transformer and active auxiliary circuit, respectively, in the simulation process. It can be observed from Fig. 10 that the DC side output voltage has 18 pulse waves during one period T_0. The parameters for the simulation validation are presented in Table 1.

Two waveforms are presented in Fig. 11 to investigate the performance of the proposed rectifier. When the compensating currents are not injected, that is, before 0.25 seconds in Fig. 11(a), the proposed rectifier operates in a conventional 18-pulse zigzag rectifier, in which the distortion of grid-side currents happens as shown in Fig. 11(b). Certainly, when the compensating currents are injected into the DC side of the previous 18-pulse rectifier, the grid-side currents waveforms of the proposed rectifier are closer to sinusoidal waves.

Fig. 12 is the spectral analysis diagram of the three-phase grid-side current i_a, whose THD is 7.68%. Obviously, when the active auxiliary circuit is not working, a conventional zigzag 18-pulse rectifier cannot meet the standards of IEEE-519 [18] and IEC 61000-3 [19] that the THD shall be lower than 5%.

When the compensating currents are injected into the DC side of the 18-pulse zigzag rectifier, according to the spectral analysis of the grid-side current i_a in Fig. 13, its THD is 1.45%, which is very small and can be lower than the harmonic requirements (by 5% for the THD of the grid-side current).

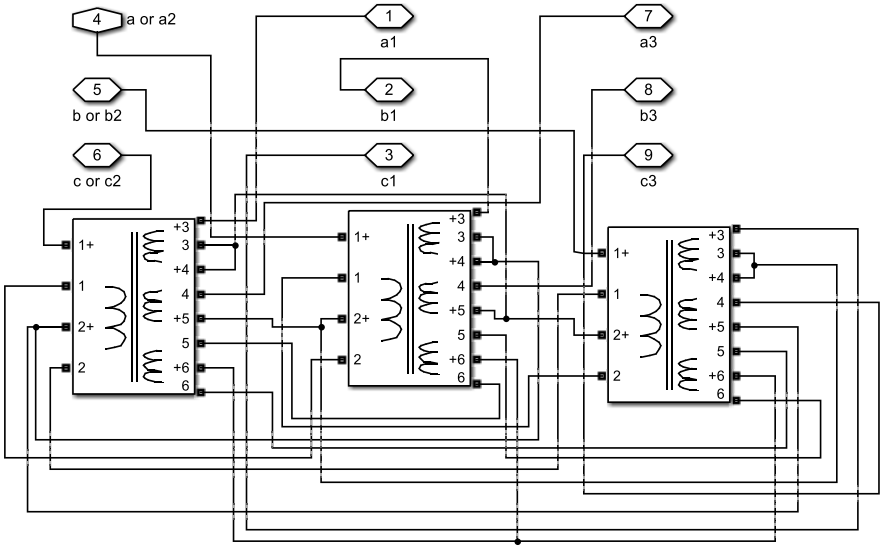

(a)

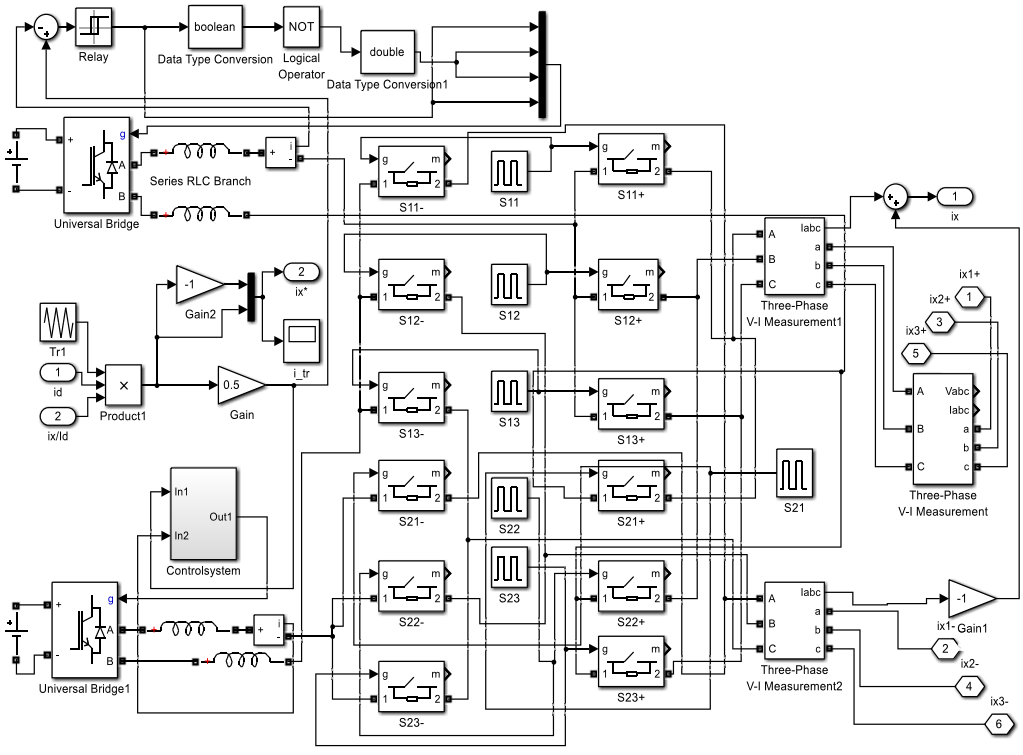

(b)

Fig. 9. Simulation model: (a) 18-pulse zigzag transformer; (b) active auxiliary circuit

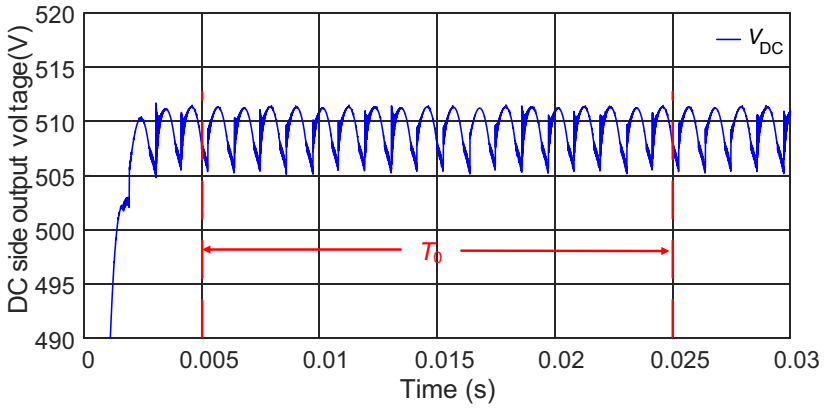

Fig. 10. DC side output voltage V_{DC}

Table 1. Parameters for simulation

Symbol	Description of parameter	Value	Unit
V_{LL}	rms value of input line voltage	380	V
$K_1 : K_2 : K_3$	Turn ratios of the windings	0.3132 : 0.1975 : 0.0201	–
R_{load}	DC load resistor	30	Ω
L_{load}	DC filter inductor	5	mH
L_x	Inverter filter inductor	40	mH
V_{DC}	DC source of inverter	500	V
f_c	Switching frequency of inverter	20	kHz
f	AC supply frequency	50	Hz
b	Current hysteresis band width	±0.01	A

According to [20], the equivalent capacity of the transformer can be calculated as follows:

$$S_{eq} = 0.5 \times \sum V_{rms} \times I_{rms}\,, \tag{23}$$

where: S_{eq} represents the equivalent capacity of the transformer; V_{rms} represents the rms value of voltage at both ends of each winding of the transformer; I_{rms} represents the rms value of the current flowing through each winding of the transformer. The rms value of currents fed to the windings of an autotransformer, IPRs and an auxiliary circuit can be obtained by the simulation model. The equivalent capacity of the zigzag autotransformer, IPRs, and the auxiliary circuit by computation is 46.30%, 10.02% and 12.21% of the output power of the load side, respectively, so the total equivalent capacity of the magnetic elements in the whole system is 68.53%.

For the intention of verifying the correctness and applicability of the proposed rectifier circuit, the proposed rectifier is compared with the 18-pulse rectifiers in [20–23] at the rated load. From

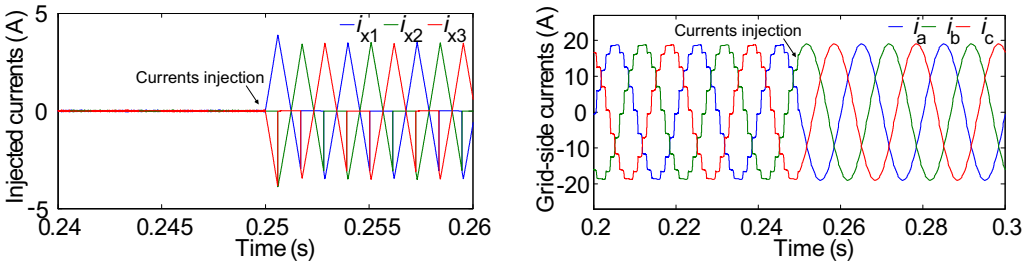

(a) (b)

Fig. 11. Two waveforms before and after the injection of the compensating currents: (a) DC side injection currents; (b) total grid-side currents i_a, i_b, i_c

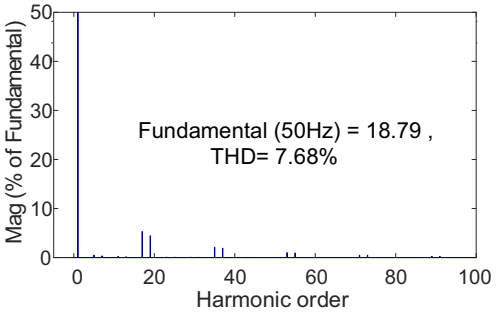

Fig. 12. Spectral analysis of i_a without currents injection

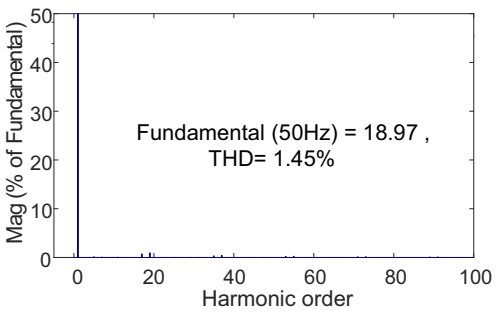

Fig. 13. Spectral analysis of i_a with currents injection

Table 2, it is observed that after the application of the DC side harmonic suppression method, the current of each winding of the rectifying system changes, which leads the equivalent capacity of the proposed rectifier to be slightly higher than that of the rectifiers in [20] and [21]. However, in terms of harmonic suppression, the THD of the grid-side current in the proposed rectifier is

Table 2. Comparison of the proposed rectifier with other 18-pulse rectifiers

Rectifier	**System configuration**	**Equivalent capacity**		**Grid-side currents THD**
		Transformer	**Total**	
[20]	18-pulse	18.00%	22.00%	8.03%
[21]	18-pulse	55.00%	55.00%	5.40%
[22]	18-pulse	–	–	3.23%
[23]	18-pulse	–	–	6.44%
Proposed	18-pulse	46.30%	68.52%	1.45%

1.45%, which is less than 8.03% of the rectifier in [20] and 5.40% of the rectifier in [21]. Besides, since the equivalent capacity is not calculated in [22, 23], from the perspective of harmonic suppression likewise, the proposed rectifier's THD of 1.45% is less than 3.23% of the rectifier in [22] and less than 6.44% of the rectifier in [23]. Therefore, the proposed 18-pulse zigzag rectifier has better performance in suppressing the grid-side current harmonics.

5. Conclusions

A low harmonic zigzag 18-pulse rectifier with an auxiliary circuit at the DC side is presented. The winding configuration of the improved zigzag autotransformer is designed. The needed DC side compensating currents are analyzed as the grid-side currents are sinusoidal. Moreover, the theoretical analysis is confirmed by the simulation of the rectifying system. The results show that when the auxiliary circuit fails or is not connected to the rectifying system, the rectifying system operates as an original 18-pulse zigzag rectifier. When the compensation currents are injected, the harmonic content of the grid-side currents can be significantly debased with the amplitude of compensation currents to be 0.24 times of the average load current I_{d}.

Acknowledgements

This work was supported by the National Natural Science Foundation of China (No. 51767013, No. 5186 7012), the Science and Technology Research and Development Plan of China Railway Corporation (No. 2017 J012-A), and the Natural Science Foundation of Gansu Province Science and Technology Department (No. 18JR3RA111).

References

[1] Yuxin L., Shiyan Y., Hongqi B., Wei Y., *A 36-pulse diode rectifier with an unconventional interphase reactor*, Energies, vol. 12, no. 5, pp. 1–18 (2019).

[2] Dongsheng Y., Shuhong W., Yilu L., *Dynamic phasor modelling of various multipulse rectifiers and a VSI fed by 18-pulse asymmetrical autotransformer rectifier unit for fast transient analysis*, IEEE Access, vol. PP, no. 99, p. 1 (2020).

[3] Saravana P., Kalpana R., Bhim S., Bhuvaneswari G., *Application of voltage multiplier in 12-pulse rectifier for sinusoidal input current*, Electronics Letters, vol. 54, no. 22, pp. 1266–1268 (2018).

[4] Rohollah A., *A simple harmonic reduction method in 20-pulse AC-DC converter*, Journal of Circuits, Systems, and Computers, vol. 28, no. 1, pp. 1950013.1–1950013.18 (2019).

[5] Fangang M., Xiaona X., Lei G., Zhongcheng M., *Dual passive harmonic reduction at DC link of the double-star uncontrolled rectifier*, IEEE Transactions on Industrial Electronics, vol. 66, no. 4, pp. 3303–3309 (2019).

[6] Xiaoqiang C., Shouwang Z., Ying W., *Simulation of a kind of active harmonic reduction 18-pulse rectifier*, Journal of Measurement Science and Instrumentation, vol. 9, no. 2, pp. 160–168 (2018).

[7] Jiarong W., Zhenghan Z., Xiaoqiang C., *Phase-shift angle analysis on 12-pulse rectifier with polygon-connected autotransformer*, Journal of the China Railway Society, vol. 42, no. 3, pp. 69–75 (2020).

[8] Jie C., Pengpeng S., Xin C., Chunying G., *Research on a novel variable step-up ratio 18-pulse auto-transformer rectifier unit*, Transactions of China Electrotechnical Society, vol. 33, no. 15, pp. 3607–3616 (2018).

[9] Fangang M., Shiyan Y., Wei Y., *Overview of multi-pulse rectifier technique*, Electric Power Automation Equipment, vol. 32, no. 2, pp. 9–22 (2012).

[10] Vidyasagar S., Kalpana R., Bhim S., *Improvement in harmonic reduction of zigzag autoconnected transformer based 12-pulse diode bridge rectifier by current injection at DC side*, IEEE Transactions on Industry Applications, vol. PP, p. 1 (2017).

[11] Fangang M., Wei Y., Shiyan Y., Lei G., *Active harmonic reduction for 12-pulse diode bridge rectifier at DC side with two-stage auxiliary circuit*, IEEE Transactions on Industrial Informatics, vol. 11, no. 1, pp. 64–73 (2015).

[12] Fangang M., Lei G., Wei Y., *Effect of circulating current on input line current of 12-pulse rectifier with active inter-phase reactor*, IET Power Electronics, vol. 9, no. 7, pp. 1398–1405 (2016).

[13] Kezhen L., Zehao C., Fangang M., Shiyan Y., *Large current rectifier and its active harmonic reduction*, Electric Machines and Control, vol. 24, no. 4, pp. 104–112 (2020).

[14] Xiaoqiang C., Shouwang Z., Ying W., *The DC-side active filter with dual-buck full-bridge inverter for wind generators*, Archives of Electrical Engineering, vol. 67, no. 2, pp. 263–277 (2018).

[15] Jiarong W., Xiaoqiang C., *Phase-shift angle analysis on zigzag autotransformer and matlab simulation*, Electrical Measurement and Instrumentation, vol. 55, no. 15, pp. 129–136 (2018).

[16] Shenghui C., Joon-Hee L., Jingxin H., Rik W., Seung-Ki S., *A modular multilevel converter with a zigzag transformer for bipolar MVDC distribution systems*, IEEE Transactions on Power Electronics, vol. 34, no. 2, pp. 1038–1043 (2019).

[17] Xiaoqiang C., Chunling H., Hao Q., *Thirty-six pulse rectifier scheme based on zigzag auto-connected transformer*, Archives of Electrical Engineering, vol. 65, no. 1, pp. 117–132 (2016).

[18] IEEE Standard 519-1992, *IEEE Guide for harmonic control and reactive compensation of static power converters*, New York: Institute of Electrical and Electronic Engineers (IEEE) (1992).

[19] International Electro-technical Commission Standard 61000-3-2, *Limits for harmonic current emissions*, Geneva: International Electrotechnical Commission (IEC) (2004).

[20] Lourenço A.C., Seixas F.J.M., Pelicer J.C., Oliveira P.S., *18-pulse autotransformer rectifier unit using SEPIC converters for regulated DC-bus and high frequency isolation*, 2015 IEEE 13th Brazilian Power Electronics Conference and 1st Southern Power Electronics Conference, Fortaleza, Brazil, pp. 1–6 (2015).

[21] Lee K., Paice D.A., Armes J.E., *The windmill topology*, IEEE Industry Applications Magazine, vol. 15, no. 2, pp. 43–53 (2009).

[22] Iwaszkiewicz J., Muc A., Mysiak P., *18-pulse rectifier in arrangement with coupled three-phase reactor*, Renewable Energy and Power Quality Journal, vol. 17, no. 1, pp. 393–397 (2019).

[23] Huaqiang Z., Quanhui L., Fangang M., Lei G., Shiyan Y., *Series-connected 18-pulse rectifier using isolated transformer*, Electric Machines and Control, vol. 23, no. 12, pp. 23–31 (2019).